International Journal of Electrical Components and Energy Conversion
2015; 1(1): 1-15
Published online March 28, 2015 (http://www.sciencepublishinggroup.com/j/ijecec)
doi: 10.11648/j.ijecec.20150101.11

Systemic Design and Optimization Improving Performances of Permanent Magnet Motors

Souhir Tounsi

National School of Electronics and Telecommunications of Sfax, Sfax University, SETIT Research Unit, Sfax, Tunisia

Email address:
souhir.tounsi@enetcom.rnu.tn

To cite this article:
Souhir Tounsi. Systemic Design and Optimization Improving Performances of Permanent Magnet Motors. *International Journal of Electrical Components and Energy Conversion.* Vol. 1, No. 1, 2015, pp. 1-15. doi: 10.11648/j.ijecec.20150101.11

Abstract: This paper describes a motor-converter systemic design methodology improving electric vehicles performances (EVP) such as: autonomy, power to weight ratio and ripple torque. This methodology takes in account of several physical, thermal and technological constraints. It rests on the coupling of a parameterized analytical model of the all motor-converter to a software based on genetic algorithms method in order to optimize parameters influencing the EVP on circulation mission in respecting several physical and technological constraints of electric vehicles. The analytical model developed covering several motor configurations is validated by the finite elements and experimental methods.

Keywords: Design, Analytic Method, Finite Element, Optimization, Electric Motor

1. Introduction

The electric vehicle constitutes a good means to improve the quality of the urban environment notably by putting an end to the chemical pollution caused by urban transportation. Nevertheless, the mass production of the electric vehicles is found again knocked to the problem of reduced autonomy that is directly linked to the problem of stored energy (battery), whose several works of research are interested there [1].

In this work we aim at optimizing the autonomy of electric vehicle, motor power to weight ratio and ripple torque from the design phase of all the motor-converter. Firstly, a stage of analytic dimensioning of the traction motor taking into account several constraints of the vehicle functioning is led in parallel with an electromagnetic modeling by the finite elements method, to gradually validate calculations. Secondly, a modeling by a finer finite elements method is realized dynamically so as to validate analytical model dimensioning all the motor-converter [1], [2]. Then, a procedure of optimization by the genetic algorithm method is developed allowing to find iteratively optimal design and control parameters of the traction chain maximizing EVP [1], [2]. The design approach is validated experimentally.

2. Studied Structures of the Traction Motor

Table 1. *Found configurations.*

Sinusoidal configurations	p	r	ν	α	β	Trapezoidal configurations	p	r	ν	α	β
1	2.n	1.5	1	2/3	1	1	2.n	1.5	1/3	1	1
2	5.n	1.2	3/2	2/3	1	2	5.n	1.2	2/3	1	1
3	2.n	1.5	1/3	3/2	2/3	3	7.n	6/7	4/3	1	1
4	5.n	1.2	2/3	3/2	2/3	4	4.n	0.75	5/3	1	1
						5	5.n	0.6	7/3	1	1

Four configurations with a sinusoidal wave-form and five configurations with a trapezoidal wave-form are found while being based on optimization rules of the ripple torque and cost. Each configuration is characterized by a variation law of the pole pairs number (p) according to an integer number n varying from one to infinity, the ratio (r) of the number of

principal teeth (N_t) by the number of pole pairs, the ratio (ν) between the angular width between two principal teeth and that of a principal tooth, the ratio (α) between the angular width of a principal tooth and that of a magnet and the ratio (β) between the angular width of a magnet and the polar step. Table 1 gives these ratios for these configurations [3].

These configurations can be with radial or axial flux. The motor structure is modular i.e. it can be with several stages. This technology allows the reduction of the production cost of these motor types. The slots are right and open what facilitates the coils insertion and reduces the motor manufacturing cost. The concentrated winding is used because of its advantages:

- Reduction of the manufacturing time of this motor (insertion of coils in one block).
- Reduction of the end-windings.
- Reduction of the motor bulk.

Figure 1 illustrates the first trapezoidal configuration (n=1) with axial flux, radial flux and only one stage [4].

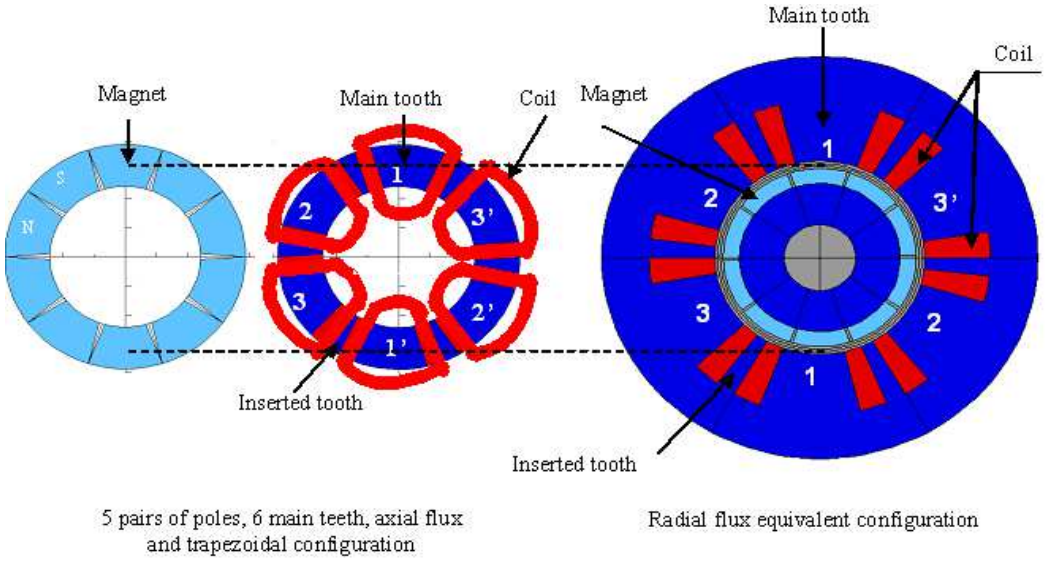

Figure 1. *First configuration (n=1).*

3. Design Methodology

The design methodology consists of the determination of geometrical and control parameters of the motor-converter improving EVP. The motor must function on a broad beach speed and without demagnetization. This methodology requires the development of an analytical and parameterized model of the all motor-converter. This latter last makes it possible to establish the relation between data, such as: the data of schedule conditions, the constant characterizing materials, the expert data, the motor configuration and the outputs such as: geometrical and electromagnetic motor magnitudes. Figure 2 illustrates the architecture of the analytical model [5], [6].

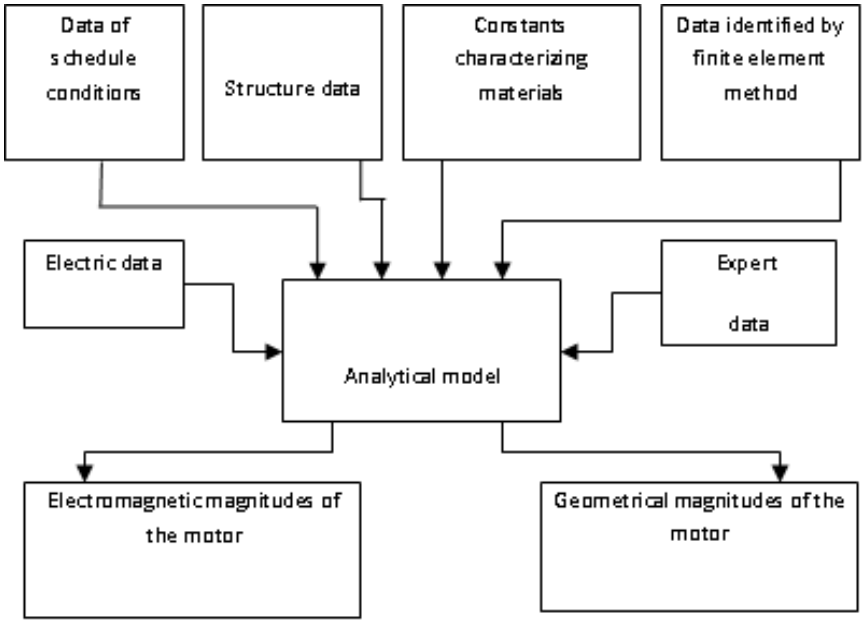

Figure 2. *Architecture of the analytical model.*

This model is validated by finite elements and experimental methods. Indeed, the motor is drawn according to its geometrical magnitudes extracted from analytical model with the software Maxwell-2d, and is simulated in dynamic and static in order to compare the results obtained with those found by the analytical method. Experimental validation is ensured by two tests [13]:

- No-load tests to test the form and the amplitude of the back electromotive force (EMF).
- Tests at load to test the form and the amplitude of the back electromotive force and the torque.

The coupling of this model to a model evaluating the EVP poses an optimization problem with several variables and constraints. This latter is solved by the genetic algorithms (GAs) method [5], [6].

The global architecture of the design methodology is illustrated in *figure 3*.

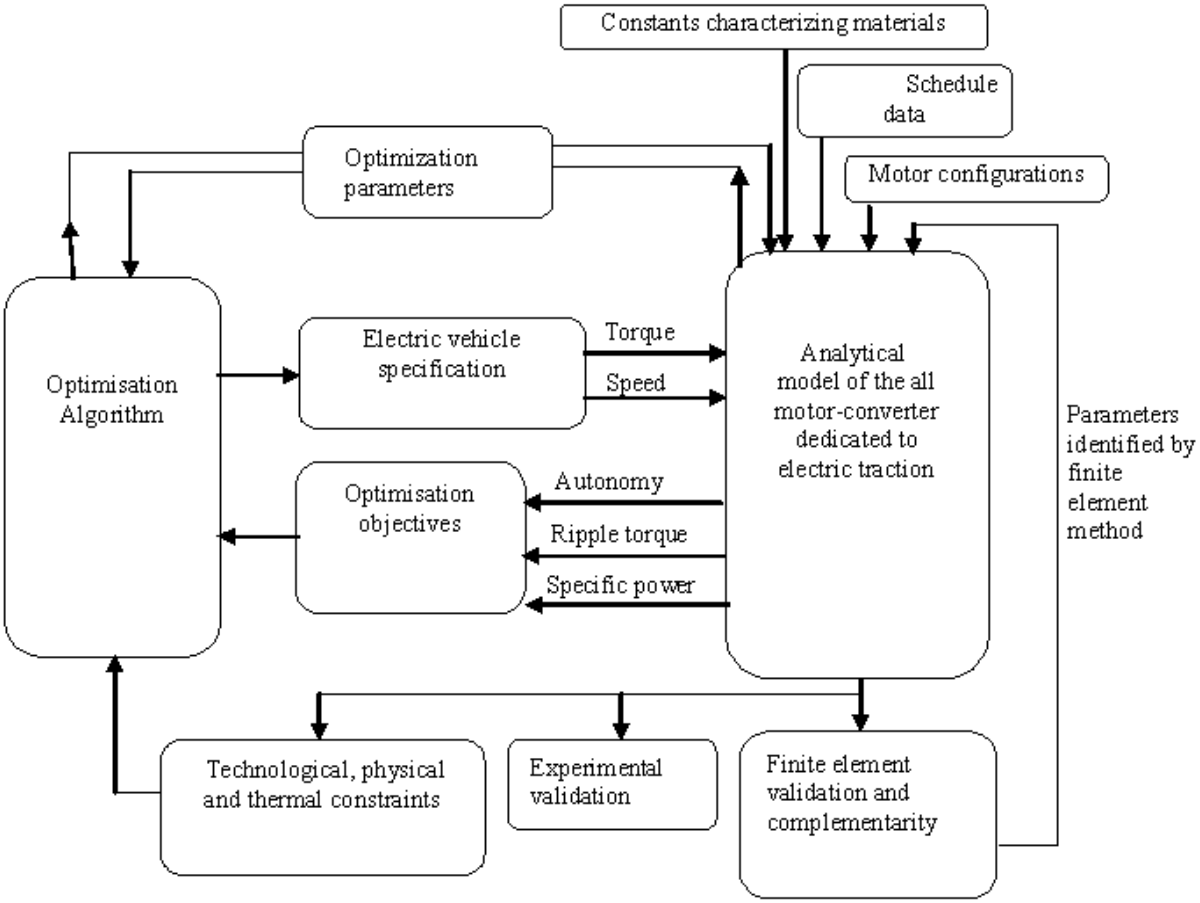

Figure 3. *Design methodology.*

4. Sizing Model of Electric Motor

The analytic sizing step is inverted starting from needs (torque, motor velocity) towards geometry dimensions. While, in classical analytic sizing, the computation starts from geometry towards needs. Indeed the limit of the plan torque/velocity of the motor is given. The electrical motor has to be able to function in this plan without constraints. Here, the problem resolution is completely reversed. For example, the operating temperature is fixed and then computed. It should be also recognised that the inversion of the problem facilitates its resolution. In the same way, the designer fixes the induction. The worksheet includes 200 items of computed elements. The difficulty is to classify these elements and to distinguish results from data [5], [6].

The worksheet computes the geometrical dimensions of rotor and stator as well as windings, temperature, inductance, leakages and efficiency for different operating points and control modes.

A sizing program is developed with equations detailed. The program inputs are:

1. Electric vehicle specifications.
2. Materials properties.
3. Configuration, i.e. magnet number and teeth number.
4. Inner and outer diameter of the motor.
5. Notebook data.
6. Current density in coils δ.
7. Rotor yoke B_{ry}, stator yoke B_{sy}, flux density in the air-gap B_g, reducer ratio and number of spire per phase N_s.

When inputs 3. and 4. are set, magnet shapes, teeth and slots are fixed. Then, the area of one tooth A_t and the average length of a spire L_{sp} are calculated from geometric equations.

4.1. Dimensioning Torque

The back electromotive force (E.m.f) stage level is given by the following expression [7], [8]:

$$E = n N_s A B \Omega \; B_g \tag{1}$$

Where N_s is the number of spire per phase, n is the module number and B_g is the flux density in the air-gap.

For the axial flux structures A and B are given by:

$$A = \frac{D_e - D_i}{2} \tag{2}$$

$$B = \frac{D_e + D_i}{2} \tag{3}$$

Where D_e and D_i are respectively the external and the internal diameter of the axial flux motor.

For the radial flux structures A and B are given by:

$$A = L_m \tag{4}$$

$$B = \frac{D_m}{2} \tag{5}$$

Where L_m and D_m are respectively the length and the bore diameter of the motor.

The instantaneous electromagnetic power $P_e(t)$ is expressed by the following relation

$$\mathrm{P_e}(t) = \sum_{i=1}^{m} \mathrm{e_i}(t)\,\mathrm{i_i}(t) \tag{6}$$

Where $e_i(t)$ and $i_i(t)$ are respectively the back electromotive force and the current of the phase i.

Two phases are fed simultaneously and the currents of phases have the same wave-form as the electromotive force with a maximum value of motor phase current I. Consequently, for a constant speed, the electromagnetic power developed by the motor takes the following form:

$$\mathrm{P_e} = 2\mathrm{EI} \tag{7}$$

The electromagnetic torque developed by the motor is expressed by:

$$T_m = 2\frac{EI}{\Omega} \tag{8}$$

The electromagnetic torque developed by the motor results [7], [8]:

$$T_m = 2\, n N_s A B B_g I \tag{9}$$

The electromagnetic torque which the motor must develop so that the vehicle can move with a speed v is deduced from the dynamics fundamental relation related to the electric vehicle dynamic:

$$T_m = \frac{P_f}{\Omega} + T_d + \left(T_b + T_{vb} + T_{fr}\right) + \frac{T_r + T_a + T_c}{r_d} + \left(\frac{J}{R_w} + \frac{M_v R_w}{r_d}\right)\frac{dv}{dt} \tag{10}$$

Where r_d is the reduction ratio, M_v is the vehicle mass, R_w is the vehicle wheel radius, J is the motor moment of inertia, v is the vehicle velocity, T_b is the rubbing torque of the motor, T_{vb} is the viscous rubbing torque of the motor, T_{fr} is the fluid rubbing torque of the motor, T_r is the torque due to the friction rolling resistance, T_a is the torque due to the aerodynamic force, T_c is the torque due to the climbing resistance, T_d is the reducer losses torque and P_f are the iron losses.

The different torques are expressed by the following equations [8]:

$$\mathrm{T_b} = \mathrm{s}\frac{\mathrm{v}}{|\mathrm{v}|} \tag{11}$$

$$\mathrm{T_{vb}} = \chi\,\mathrm{v} \tag{12}$$

$$\mathrm{T_{fr}} = \mathrm{k}\;\mathrm{v}|\mathrm{v}| \tag{13}$$

$$T_r = R_w f_r M_v g \tag{14}$$

$$T_a = R_w \frac{\left(M_{va} C_x A_f\right)}{2} V^2 \tag{15}$$

$$T_c = M_v g \sin(\lambda) \tag{16}$$

Where s is the dry friction coefficient, χ is the viscous friction coefficient, k is the fluid friction coefficient, λ is the angle that the road makes with the horizontal, M_{va} is the density of the air, C_x is the aerodynamic drag coefficient, r_p is a coefficient taking account of the mechanical losses in the motor and the transmission system, and A_f is the vehicle frontal area. The phase current becomes:

$$I = \frac{T_m}{2 n N_s A B B_g} \tag{17}$$

The dimensioning current is expressed as follows:

$$I_{\mathrm{dim}} = \frac{T_{\mathrm{dim}}}{2 n N_s A B B_g} \tag{18}$$

T_{dim} is the dimensioning torque. This torque is found by the genetic algorithm method on a standardized circulation mission in order to not exceed the limiting temperatures and to minimize the motor mass.

Several methods were proposed to define dimensioning sizes of the motor-reducer torque, based on simplified statistical tools [8]. A first method is based on the determination of the effective torque for a circulation mission in order to take into account the thermal aspect [9]. A second more elaborate approach consists in defining zones of strong occurrences and to take the sizes resulting from these zones like dimensioning sizes. Finally, a last simpler method consists in dividing the torque-speed plan into 4 zones, to take the gravity center of each zone then to consider the gravity

center of these four points balanced by the number of each zone points as dimensioning point. These methods have the advantage of quickly providing useful sizes for dimensioning and simulation, nevertheless they do not take into account the problem of electric vehicle consumption minimization. For our approach, the dimensioning torque will be iteratively calculated by the genetic algorithms method in order to satisfy a global optimization of autonomy while respecting the dimensional thermal stresses relating to our application specified by the schedule of conditions. To guide the algorithm to converge towards a powerful solution and in order to limit the space of research, the motor dimensioning torque must satisfy the following condition extracted inequality:

$$(1-\varepsilon)R_w\left(\frac{\frac{J}{R_w^2}+\frac{M_v}{r_d}}{t_d}V_b+\frac{M_v g\sin(\lambda)}{r_d}\right)\le T_{\dim}\le(1+\varepsilon)R_w\left(\frac{\frac{J}{R_w^2}+\frac{M_v}{r_d}}{t_d}V_b+\frac{M_v g\sin(\lambda)}{r_d}\right) \quad (19)$$

The adjustment coefficient of the torque ε generally does not exceed 0.25 and will be adjusted by simulations of the propulsion system on normalised circulation missions.

Figure 4 illustrates the evolution of motor torque in versus vehicle speed for a reducing ratio equal to 3.

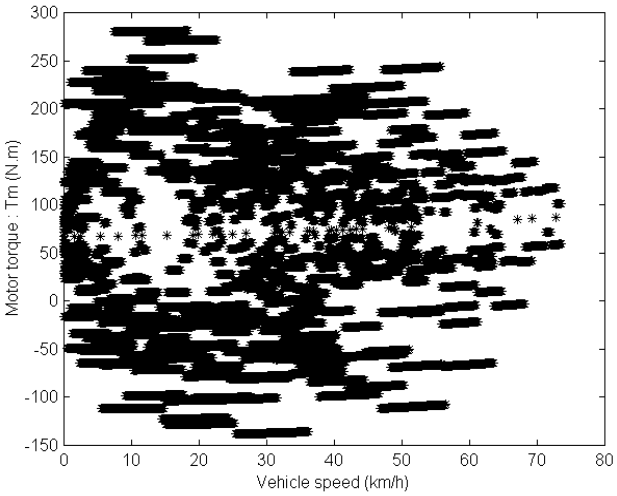

Figure 4. *Motor torque evolution in versus electric vehicle speed.*

This figure shows that the dimensioning torque is around 250 Nm, which validates inequality 19.

4.2. Converter's Continuous Voltage for Trapezoidal Wave-Form Motor Structures

The motor constant is defined by:

$$K_e=2nN_s ABB_g \quad (20)$$

The converter's continuous voltage U_{dc} is calculated so that the vehicle can function at a maximum and stabilized speed with a weak torque undulation. The electromagnetic torque that the motor must exert at this operation point, via the mechanical power transmission system T_{Udc} (reducing + differential) is estimated by the following expression [7], [8]:

$$T_{Udc}=\frac{P_f}{\omega}+T_d+\left(T_b+T_{vb}+T_{fr}\right)+\frac{T_r+T_a+T_c}{r_d} \quad (21)$$

At this operation point, the phase current is given by the following relation:

$$I_p=\frac{T_{Udc}}{K_e} \quad (22)$$

The only possibility making it possible to reach the current value I_p with a reduced undulation factor (10% for example) is to choose the converter's continuous voltage solution of the following equation [10]:

$$r=\frac{t_m}{t_p}=10\% \quad (23)$$

Where t_p is the phase current maintains time at vehicle maximum speed and t_m is the boarding time of the phase current from zero to I_p [10]:

$$t_m=-\frac{L}{R}\ln\left(1-\frac{2RI_p}{U_{dc}-K_e\Omega_{\max}}\right) \quad (24)$$

Where R and L are respectively the phase resistance and inductance and Ω_{max} is the maximum angular velocity of the motor.

The phase current maintains time at maximum speed of vehicle (corresponds to 120 electric degrees) is given by the following formula [10]:

$$t_p=\frac{1}{3}\frac{2\pi}{p\Omega_{\max}} \quad (25)$$

Figure 5 illustrates the PWM energize principle of trapezoidal wave-form configuration.

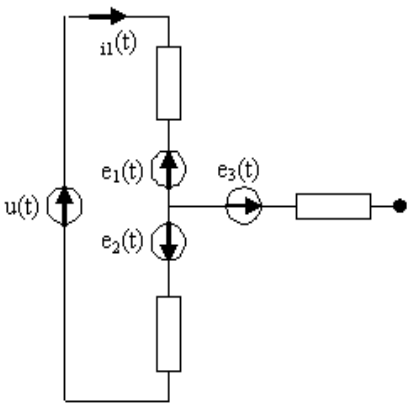

Equivalent diagram during the first 60 degrees

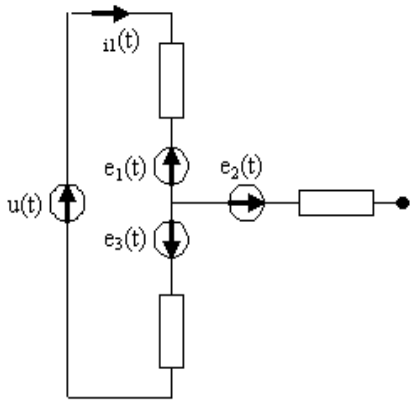

Equivalent diagram during the second 60 degrees

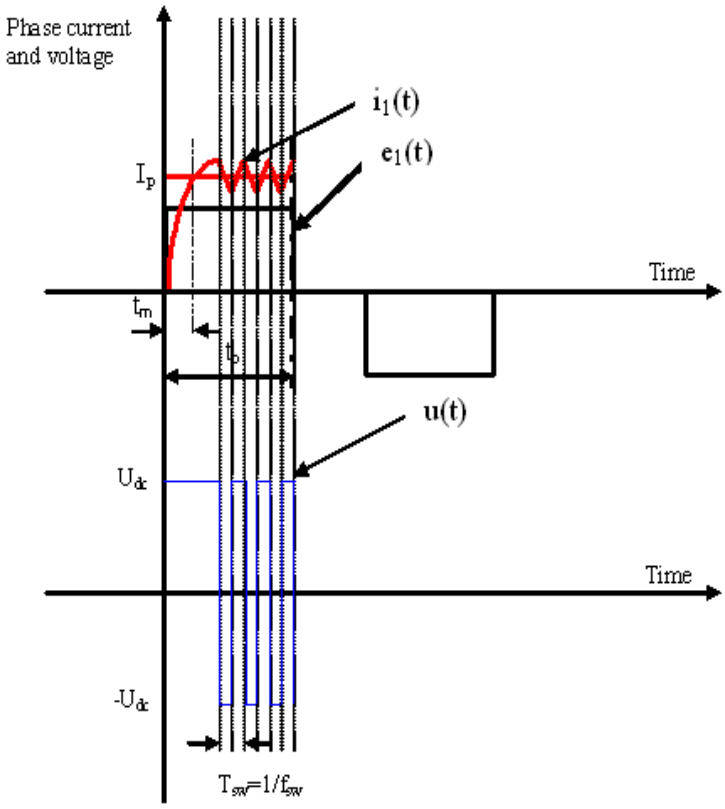

Figure 5. *PWM energize principle of trapezoidal wave-form configuration.*

The converter's continuous voltage takes the following form:

$$U_{dc}=\frac{2RI_p}{1-\exp\left(-\frac{2\pi r}{3p\Omega_{\max}\frac{L}{R}}\right)}+K_e\Omega_{\max} \quad (26)$$

The phase inductance of the all configurations is expressed as follows:

$$L=\mu_0\times\left(\frac{\frac{A_t}{2}}{2\times(g+t_m)}+\frac{Ah_s}{A_s}\right)\left(\frac{N_s}{\frac{N_t}{3}}\right)^2\times\frac{N_t}{3} \quad (27)$$

Where μ_0 is the air permeability, A_t is slot area, t_m is the magnet thickness, h_s is slot height, g is the air-gap thickness and A_s is the slot width.

Figure 6 illustrates the converter's continuous voltage evolution in versus vehicle speed.

The converter continuous voltage increases by increasing the vehicle speed which validates the fact of calculating its value at maximum speed. Two important factors involving the increase of the converter continuous voltage:

- The increase of the motor electric constant.
- The reduction of the undulation factor.

Consequently, a compromise between the reduction of the converter continuous voltage directly related to the space reserved for the battery and the reduction of undulation factor is to be found.

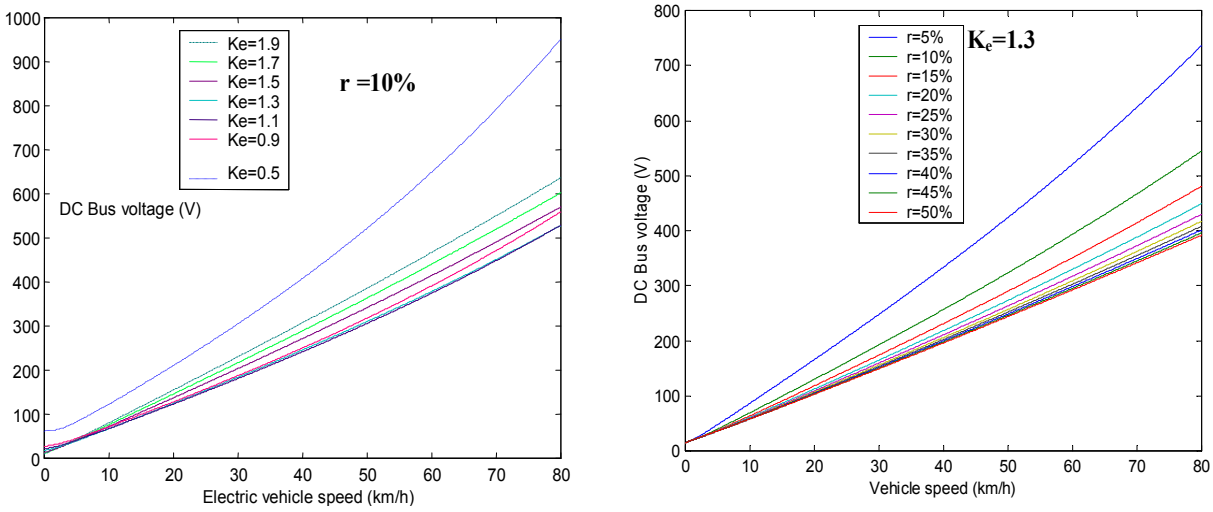

Figure 6. *Converter's continuous voltage evolution in versus vehicle speed.*

4.3. Converter's Continuous Voltage for Sinusoidal Wave-Form Motor Structures

The maximum value of the back E.m.f. is given by the following expression:

$$E = nN_s A B \Omega \ B_g \tag{28}$$

For an energize with current of maximum amplitude I and in phase with the back E.m.f., the electromagnetic torque developed by the motor takes the following form [4], [5]:

$$T_m = \frac{3}{2}\frac{EI}{\Omega} \tag{29}$$

The torque developed by the motor results:

$$T_m = \frac{3}{2} nN_s A B B_g I \tag{30}$$

The electric constant of the motor is defined by:

$$K_e = \frac{3}{2} nN_s A B B_g \tag{31}$$

The maximum value of the back E.m.f takes the following form [4]:

$$E = \frac{2}{3} K_e \Omega \tag{32}$$

The electromagnetic torque becomes:

$$T_m = K_e I \tag{33}$$

The motor must develop the torque defined at maximal speed. It is ordered to full wave when it reaches its maximal speed. Forms of phase voltages are illustrated in figure 7.

The first harmonic of the phase 1 voltage is given by the following expression:

$$U_{ph11} = \frac{2U_{dc}}{\pi} \sin\left(\frac{2\pi}{T} t + \phi\right) \tag{34}$$

To have a maximal torque, the motor is operated with a power factor $f_p = 1$. The diagram of Behn Eschemburg for this operating mode is given by figure 8.

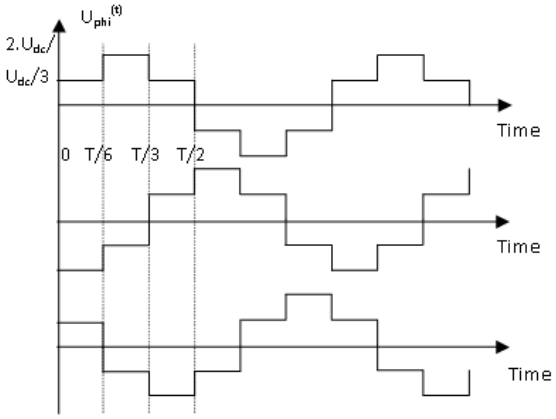

Figure 7. *Forms of phase voltages.*

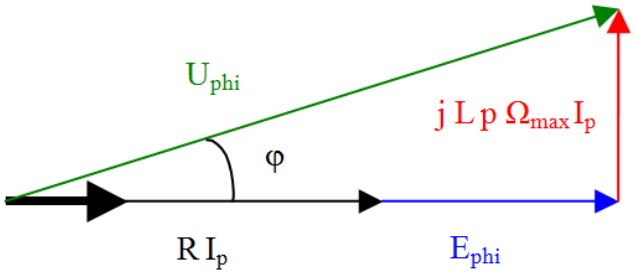

Figure 8. *Diagram of Behnhemburg.*

The phase model of Behn Eschemburg is given by the following relationship:

$$\overline{U_{phi}} = \overline{E_{phi}} + R\overline{I_p} + jLp\Omega\overline{I_p} \tag{35}$$

The maximal value of the first harmonic of the phase voltage at maximal speed is deduced from:

$$U_{phi} = \sqrt{\left(RI_p + E_{phi}\right)^2 + \left(Lp\Omega_{\max} I_p\right)^2} \tag{36}$$

The voltage of the DC bus is deduced from (35) and (36):

$$U_{dc} = \frac{\pi}{2}\sqrt{\left(RI_p + E_{phi}\right)^2 + \left(Lp\Omega_{\max} I_p\right)^2} \tag{37}$$

E_{phi} is the maximal value of the back E.m.f. at the maximal speed:

$$E_{phi} = \frac{2}{3}K_e\Omega_{\max} \tag{38}$$

5. Motor sizing

For the all configurations of the motor the magnet thickness should be equal to [4]:

$$t_m = \mu_m \frac{B_g}{B_r - \frac{B_g}{K_{fu}}} g \tag{39}$$

Where μ_m is the magnet's relative permeability, B_r is the remanence, $K_{fu} < 1$ is the magnet's leakage coefficient and g is the air-gap thickness.

To avoid demagnetization, the phase currents should be expressed as follows [4]:

$$I_d = \left(\frac{B_r - B_{\min}}{\mu_m} t_m - B_{\min} K_{fu} g\right) \frac{p}{2\mu_0 N_s} \tag{40}$$

Where B_{min} is the minimum flux density allowed in the magnets and μ_0 is the air permeability. The rotor yoke thickness t_{ry} and stator yoke thickness t_{sy} derive from the flux conservation [4], [5]:

$$t_{ry} = \frac{B_g}{B_{ry}} \frac{Min\left(A_t, A_m\right)}{2A} \frac{1}{K_{fu}} \tag{41}$$

$$t_{sy} = \frac{B_g}{B_{sy}} \frac{Min\left(A_t, A_m\right)}{2A} \tag{42}$$

Where A_t is the tooth area, A_m is the area of one magnet, B_{ry} and B_{sy} are respectively the flux densities in rotor and stator yokes. For the axial flux and trapezoidal wave-form motor configurations the slot height is [4], [5]:

$$h_s = \frac{3.2.N_s}{2N_t} \frac{I_{\dim}}{\delta} \frac{1}{K_f} \frac{1}{A_s} \tag{43}$$

For the axial flux and sinusoidal wave-form motor configurations the slot height is:

$$h_s = \frac{3.2.N_s}{2N_t} \frac{I_{\dim}}{\sqrt{2}\,\delta} \frac{1}{K_f} \frac{1}{A_s} \tag{44}$$

For the radial flux and trapezoidal wave-form motor configurations the slot height is:

$$h_s = \sqrt{\frac{2I_{\dim} N_s}{N_t \delta K_f A_s} + \left(\frac{D_m}{2} + \frac{g}{2}\right)^2} - \left(\frac{D_m}{2} + \frac{g}{2}\right) \tag{45}$$

As For the radial flux and sinusoidal wave-form motor configurations the slot height is expressed by:

$$h_s = \sqrt{\frac{2I_{\dim} N_s}{\sqrt{2}N_t \delta K_f A_s} + \left(\frac{D_m}{2} + \frac{g}{2}\right)^2} - \left(\frac{D_m}{2} + \frac{g}{2}\right) \tag{46}$$

Where N_t is the number of principal teeth, δ is the current density in slots, K_f is the slot filling factor, A_s is the slot width and I_{dim} is the dimensioning current:

$$I_{\dim} = \frac{T_{\dim}}{K_e} \tag{47}$$

The slot width is expressed as follows:

$$A_s = B\ SIN\left(\frac{1}{2}\left(\frac{2\pi}{N_t} - \alpha\beta\frac{\pi}{p}\left(1 - r_{did}\right)\right)\right) \tag{48}$$

Where r_{did} is the ratio between the angular width of the inserted tooth and that of the principal tooth. This ratio is optimised by finite elements simulations in order to reduce the flux leakages and to improve the back E.m.f. wave-form.

6. Power to Weight Ratio

The power to weight ratio P_{wr} is defined by the ratio between the motor rated power and the motor weight W_m:

$$P_{wr} = \frac{R_w\left(\frac{J}{R_w^2} + \frac{M_v}{r_d}}{t_d} V_b + \frac{M_v g \sin\left(\lambda\right)}{r_d}\right) \frac{V_b}{R_w} r_d}{W_m} \tag{49}$$

The motor weight is expressed as follows:

$$W_m = W_{sy} + W_t + W_c + W_{ry} + W_m \tag{50}$$

For the axial flux configurations the weight of stator yoke W_{sy}, tooth W_t, copper W_c, rotor yoke W_{ry}, and magnets W_m are expressed as follows:

$$W_{sy} = nd\frac{\pi}{4}\left(D_e^2 - D_i^2\right)t_{sy} \tag{51}$$

$$W_t = nd\ N_t A_t h_s \tag{52}$$

$$W_c = 3n N_s L_{sp} \frac{I_{\dim}}{\delta} d_c \tag{53}$$

$$W_{ry} = \pi \left(\left(\frac{D_e}{2} \right)^2 - \left(\frac{D_i}{21} \right)^2 \right) t_{ry} d \tag{54}$$

$$W_m = 2n\, p A_m t_m d_m \tag{55}$$

For the radial flux configuration the weight of stator yoke W_{sy}, tooth W_t, copper W_c, rotor yoke W_{ry}, and magnets W_m are expressed as follows:

$$W_{sy} = n\pi \left(\left(\frac{D_m}{2} + \frac{g}{2} + h_s + t_{sy} \right)^2 - \left(\frac{D_m}{2} + \frac{e}{2} + h_s \right)^2 \right) L_m d \tag{56}$$

$$W_t = n \frac{A_d}{2} N_t \left(\left(\frac{D_m}{2} + \frac{g}{2} + h_s \right)^2 - \left(\frac{D_m}{2} + \frac{g}{2} \right)^2 \right) L_m d \tag{57}$$

$$W_c = 3n \left(2L_m + 2\left(A_e + A_d \right) \left(\frac{D_m}{2} + \frac{g}{2} + \frac{h_s}{2} \right) \right) \times N_s \left(\frac{I_{\dim}}{\sqrt{2}\delta} \right) d_c \tag{58}$$

$$W_{ry} = \pi n \left(\left(\frac{D_m}{2} - \frac{g}{2} - t_m \right)^2 - \left(\frac{D_m}{2} - \frac{g}{2} - t_m - t_{ry} \right)^2 \right) L_m d \tag{59}$$

Where d is the density of the metal sheet, d_c is the density of copper, d_m is the magnet density, A_a is the magnet angular width, A_d is the angular width of principal teeth and A_e is the slot angular width.

7. Motor Losses

For the trapezoidal wave-form configurations, the copper losses are expressed by the following relation:

$$P_c = 2RI^2 \tag{60}$$

For the sinusoidal wave-form configurations, the copper losses are expressed by the following relation:

$$P_c = 3R \left(\frac{I}{\sqrt{2}} \right)^2 \tag{61}$$

The phase resistance is given by the following expression:

$$R = r_{cu}\left(T_b \right) \frac{N_s L_{sp}}{S_c} \tag{62}$$

Where r_{cu} is the copper receptivity, L_{sp} is the average length of spire, T_b is the copper temperature and S_c is the active section of one conductor:

$$S_c = \frac{I_{\dim}}{\delta} \tag{63}$$

The iron losses are expressed by the following relation [4], [5]:

$$P_{fer} = C\ f^{1.5} \left(n W_t B_g^2 + n W_{sy} B_{sy}^2 \right) \tag{64}$$

Where c is the core loss, f is the motor powering frequency, W_t is the teeth weight, W_{sy} is the stator yoke weight, B_g is the airgap flux density and B_{sy} is the flux density in stator yoke. The mechanical losses are expressed by the following relation [7]:

$$P_m = \left(T_b + T_{vb} + T_{fr} \right) \Omega \tag{65}$$

Where Ω is the angular speed of the electric motor. Configuration selection

In the framework of our application, the interval of variation of the number of pair poles is delimited by the proportional powering frequency to the motor velocity.

On the one hand and knowing that the maximal commutation frequency of the converter the motor is fixed to 8000 Hz because of the actual technology, we will limit the powering frequency of the converter to 533 Hz in order to preserve a ratio of 15 between the frequency of modulation and the frequency of motor functioning [9], [10], [11], [12], [13] .

On the other hand and under these assumptions of using a reducer in the mechanical transmission chain, the value of reduction ratio can't exceed 8. Under these assumptions, the maximal velocity of the wheel takes 80 km/h and the value of p must be 5 for a reduction ratio equal to 8.

A three-phase motor with 4 pair poles, axial flux and trapezoidal wave-form is chosen from the second configuration to resolve the electric vehicle traction problem (Figure 3). Each winding is formed by two diametrically opposite coils, each of them is inserted around a main tooth in order to reduce the flux leakages.

The motor is designed to be inserted in a wheel of an electric vehicle. Consequently, the outer diameter of the motor is limited by the vehicle wheel diameter. Thus, the choice of the winding is a fundamental factor of progress in the selected solution. Indeed, the concentrated winding allows to reduce significantly the end windings and thus to increase the active part volume. The motor performances are increased for a given bulk. Furthermore, the concentrated winding is easy to manufacture compared to a classical overlapping winding.

The manufacturing time of the winding is strongly reduced and the automation of winding can be more easily carried out compared to a classical overlapping winding. This last point

has a great economic importance for the motor designed for mass production.

8. Converter Model of the Selected Configuration

The motor is supplied with a reversible current three-phase converter to ensure the energy recuperation during the deceleration phases (figure 9). It is fed by current crenels of 120 electric degrees. The motor supply rises then in a succession of sequences of 60 electric degrees during which two phases are fed in series by a constant current I.

The resulting torque seems a simple juxtaposition of the torque relating to the different windings. The adjustment of current in the motor is ensured by pulse width modulation (PWM). Two types of modulation exist, the modulation with two transistors and the modulation with only one transistor [10], [11], [12], [13].

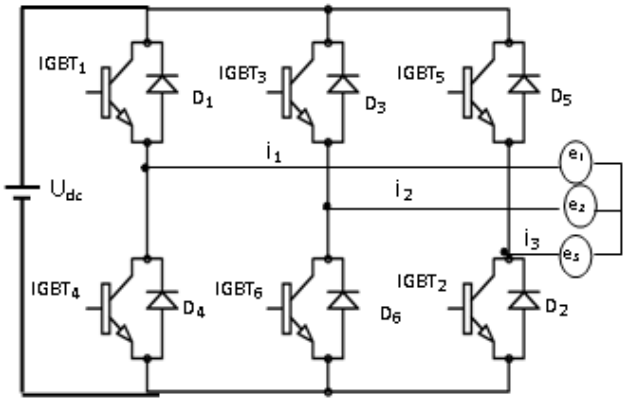

Figure 9. *Converter structure.*

If it is supposed that phase 1 and 2 are fed, during the first half period of modulation, transistor IGBT1 and IGBT6 lead and the two phases of the motor will be fed by an increasing current. During the second half period of modulation, these two transistors are forced with blocking, as a consequence the diodes D_4 and D_3 lead and the two phases of the motor will be fed by a decreasing current.

For a modulation with two transistors, the conduction losses are expressed by the following formula:

$$P_c = 2\left(\rho V_{ce}(I) I + (1-\rho) V_d(I) I\right) \quad (66)$$

Where ρ is the cyclic ratio, V_{ce} is the transistor collector-emettor voltage and V_d is the terminal voltage of the diode.

The commutation losses are expressed as follows:

$$P_{com} = 2\left(K_{Eon} E_{on}(I) + K_{Eoff} E_{off}(I)\right) f_{sw} \quad (67)$$

Where K_{Eon} is expressed as follows:

$$K_{Eon} = K_{Eoff} = \frac{U_{dc}}{E_w} \quad (68)$$

Where E_{on} and E_{off} are respectively the energy dissipated by commutation at the closing of the IGBT and the energy dissipated by commutation at the opening of the IGBT and E_w is the test voltage.

For the modulation with only one transistor, during the first half period of modulation the transistors IGBT1 and IGBT6 lead and the motor is thus supplied by an increasing current. During the second half period of modulation transistor IGBT1 is forced to blocking, as a consequence the D4 diode starts and the IGBT6 transistor remains conducting, the motor is thus supplied by a decreasing current.

The conduction losses deduced from this functioning mode are expressed as follows:

$$P_{con} = (1+\rho) V_{ce}(I) I + (1-\rho) V_d(I) I \quad (69)$$

And the losses by commutation are expressed by the following formula:

$$P_{com} = \left(K_{Eon} E_{on}(I) + K_{Eoff} E_{off}(I)\right) f_{sw} \quad (70)$$

At stabilized speed, the current is controlled around a constant current $I_0 \pm \Delta I$ to reduce the torque undulation developed by the electric motor. ΔI must be the weakest possible. This leads to an increase in the switched frequency and consequently to an increase in the commutation losses. A compromise between the reduction of the losses and the reduction of the torque undulation is to be found. The first type of modulation is more adapted to frequencies raised considering the current is to control under a voltage rocking between +Udc and - Udc, while the second type is adapted for low frequencies considering than the current is controlled under a voltage rocking between +Udc and 0. In this work we retained the second type of modulation leading to losses in the inverter significantly more reduced compared to those due to the first type of modulation.

9. Reducer Model

The reducer is used with the aim of reducing the motor dimensioning torque and as a consequence its mass and its cost. Figure 10 represents two combined profiles P_1 and P_2 in contact in a point of the action line:

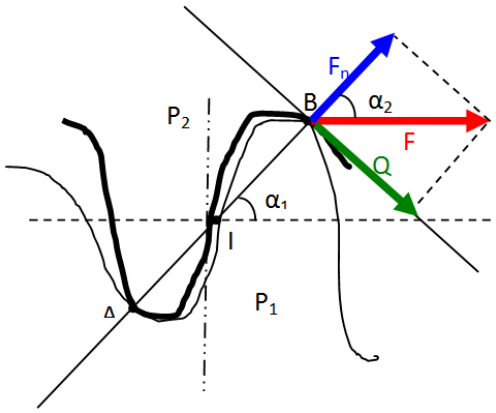

Figure 10. *Two combined profiles P_1 and P_2 in contact in a point of the action line.*

The reducer losses torque is given by [11]:

$$T_d = \left(f\left(\frac{1}{r_1} \pm \frac{1}{r_2} \right) \frac{g_f^2 + g_a^2}{2(g_f + g_a)\cos\alpha_1} \right) T_m \quad (71)$$

Where r_1 and r_2 are respectively the radius of the driving reducer wheel and the radius of carried out reducer wheel, g_f is the length of approach, g_a is the length of the retirement.

The losses in the reducer are givenby the following expression:

$$P_r = \left(1 - f\left(\frac{1}{r_1} \pm \frac{1}{r_2} \right) \frac{g_f^2 + g_a^2}{2(g_f + g_a)\cos\alpha_1} \right) T_m \omega \quad (72)$$

10. Average Model of Autonomy

The average autonomy on a circulation mission is expressed as follows:

$$Au = \frac{\left(E_b - |E_r|\right) \frac{1}{T} \int_0^T \eta(t)\, dt}{P_{um1}} v_m \quad (73)$$

Where E_b is the energy stored in the battery, E_r is the energy to recover by braking, v_m is the average velocity of the circulation mission, P_{um1} is the average value of the power provided by the motor, T is the circulation mission duration and η is the power train efficiency. The useful power in the wheels will be expressed by:

$$P_u = \begin{pmatrix} r_d \left(\frac{P_f}{\Omega} + T_d + \left(T_b + T_{vb} + T_{fr} \right) \right) + \\ T_r + T_a + T_c + \left(\frac{r_d J}{R_w} + M_v R_w \right) \frac{dv}{dt} \end{pmatrix} \frac{v}{R_w} \quad (74)$$

P_u is the sum of two powers, one positive P_{u1} in this case it is provided by the motor and the other negative P_{u2}, and it is recovered.

$$\eta(t) = \frac{P_{u1}(t)}{P_g(t)} \quad (75)$$

Where $P_g(t)$ is the battery generated power. This power is expressed as follows:

$$P_g(t) = P_{u1}(t) + P_b(t) + P_c(t) + P_{com}(t) + P_m(t) + P_j(t) + P_f(t) + P_r(t) \quad (76)$$

Where P_b is the battery losses:

$$P_b = R_b I^2 \quad (77)$$

Where R_b is the internal resistance of the battery. This resistance is identified in experiments by two tests:

- Test at no-load to determine the E.m.f.
- Test on resistive load to determine R_b.

The average power at the wheels is given by the following expression:

$$P_{um1} = \frac{1}{T} \int_0^T P_{u1}\, dt \quad (78)$$

The vehicle average velocity is given by:

$$v_m = \frac{1}{T} \int_0^T v(t) dt \quad (79)$$

The energy recovered by braking on one mission of circulation is given by:

$$E_r = \int_0^T P_{u2}(t) dt \quad (80)$$

The average model of autonomy is implanted under MATLAB/SIMULINK.

11. Finite Element Modeling of Traction Motor

Modeling by finite elements is a study of adjustment and also a stage of validation. The finite elements analysis of the axial flux synchronous motors is naturally a three-dimensional problem but a transformation is applied to have a two-dimensional model of which the use is more malleable and also faster. A parameterized model including many parameters is then developed.

11.1. Cylindrical Cut Plan Transformation

The engine can be studied in 2D by decomposition in cylindrical plans of cuts which produce different models. This choice is made in order to reduce the time of simulation. The variation of surface in glance enters a magnet and a principal tooth is not perfectly linear because of the principal edges. To find the true variation of flux, it is necessary to study the motor on several plans of cylindrical cuts. But it was shown that non-linearity coming from the variation of surface in glance enters a magnet and a principal tooth is very low for the structure.

Another simplification consisting in supposing that the magnetic material is linear was validated.

In conclusion, the motor is studied on an average contour with simulations into linear.

11.2. Axial/Radial Transformation

The motor with axial flux is studied by its equivalent with radial flux. The transformation is carried out on an average contour of the engine with axial flux. To have the same back E.m.f., it is necessary that the average diameter of the axial structure is equal to the average diameter of the motor with radial flux ($D_m = (D_e+D_i)/2$), and the length of the radial motor L_m is equal to $(D_e-D_i)/2$ [6].

It should be noted that to have the same magnetic flux densities in the various zones of the two structures, it is necessary that these last have the same thickness of magnet, same thickness of stator and rotor yoke and the same height of teeth.

11.3. Finite Elements Model

The mesh of the air-gap is achieved in three layers. This increase of the number of nodes is necessary to have a good temporal representation. The finite elements problem is solved by using the Maxwell-2D program. The solver allows the use of external electric circuits.

The distribution of the flux lines when the motor operates at no-load is illustrated in figure 11.

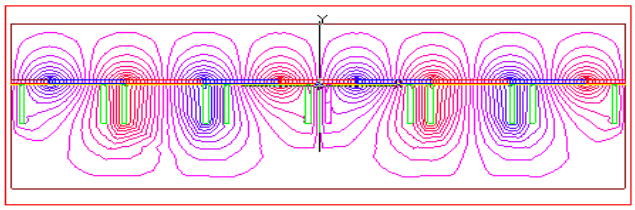

4 pairs of poles, 6 main teeth and axial trapezoidal ave-form structure

5 pairs of poles, 6 main teeth and radial trapezoidal wave-form structure

Figure 11. *Filed lines at no-load.*

11.4. Simulation Results

The flux at load for the motor with trapezoidal wave-form is illustrated by the figure 12:

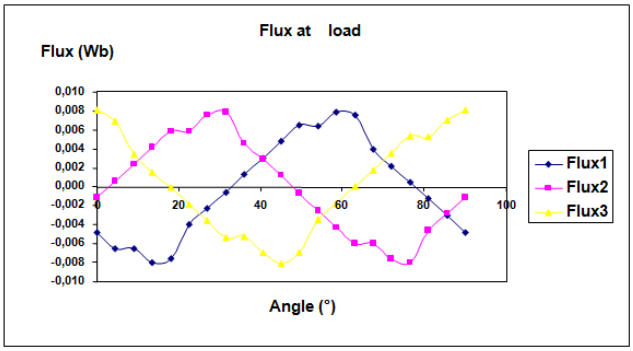

Figure 12. *Flux at load for the motor with tarpezoïdal wave-form.*

The electromotive forces (Emf) at load for the motor with Trapezoidal wave-form is illustrated by the figure 13 [6]:

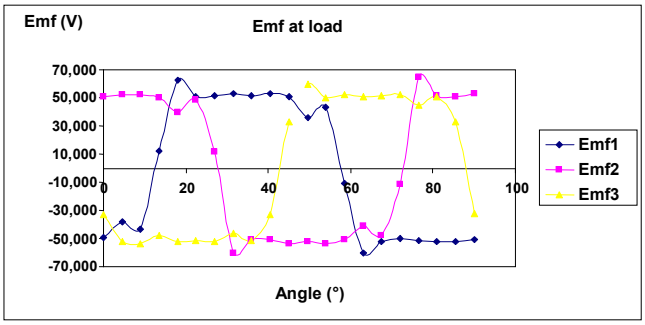

Figure 13. *Emf at load for the motor with trapezoidal wave-form.*

The E.m.f. value achieves its value calculated by analytical model which validates entirely this dimensioning method.

11.5. Model of the Inductance

The inductance value is usually low for this type of machine because the flux created by the coil must cross the air-gap and the magnet thickness. In order to compute the inductance, the motor is supplied by its peak current and the magnets are replaced by air [6]. The flux lines distribution around one stator pole are illustrated by figure14.

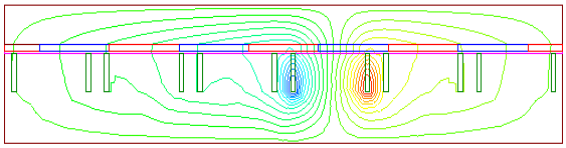

Figure 14. *Flux lines distribution around one stator pole.*

The machine air-gap is relatively large producing then important flux leakages in slots. For a linear system, the inductance value of a phase constituted by two coils may be obtained from:

- The energy calculation:

$$L = \frac{2}{I^2} A \iint_{area} B_m H ds \qquad (81)$$

- The flux calculation:

$$L=\frac{N_s}{I}\frac{1}{s_{slot}}A\int A_s\,ds \tag{82}$$

Where B_m is the flux density, H is the magnetic field, s_{slot} is the slot area and A_s is scalar potential.

The finite elements analysis valid the analytic model of inductance. The mutual inductance is calculated with the same method by calculating the flow sensed by the adjacent coil of the coil supplied.

12. Experimental Validation of the Design Methodology

A prototype of motor sized by the combined method finite elements / analytic is manufactured for the purpose to test the validity of this method. The stator of this motor is illustrated by the figure 15.

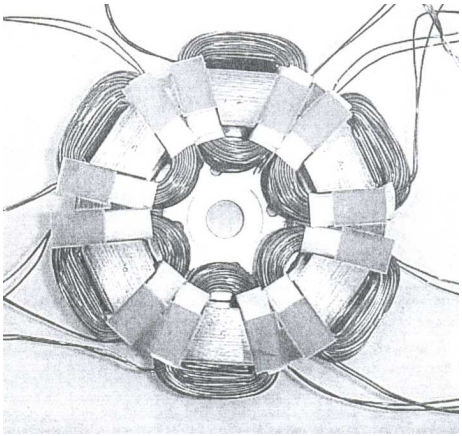

Figure 15. *Stator of the manufactured prototype.*

Two experimental tests of the motor are realized so as to test the validity of the sizing method [13].

- The first consists in involving the motor by an asynchronous motor to its nominal speed. The wave-form of the electromotive force at no load visualized on a numerical oscilloscope is very close to that calculated by the finite elements method. The landing level of the electromotive force has reached the value given by the sizing method, with an error of 2 %.
- The second consists in powering the motor by its nominal current, by the intermediary of a PWM converter. The measured torque reaches the value calculated by the analytic method with an error of 2.4%.

Genetic algorithms optimisation of EVP

The EVP model is expressed by the following expression:

$$EVP=A_u+a\,P_{wr} \tag{83}$$

Where "a" is a coefficient fixing the influence degree of P_{wr} at the global objective function compared to A_u. Indeed, "a" brings closer the value of (a P_{wr}) to the value of A_u.

The optimisation problem consists in optimising the EVP with respect to the problem constraints. In fact, Genetic Algorithms (GAs) are used to find optimal values of the switched frequency f_{sw} , radius of the wheel in meters R_w, the gear ratio r_d, the internal diameter D_i, the external diameter D_e, the flux density in the air-gap B_g, the current density in the coils δ, the flux density in the rotor yoke B_{ry} , the flux density in the stator yoke B_{sy} and the number of phase spires N_s[15], [16], [17], [18].

The beach of variation of each parameter $x_i \in$ (f_{sw} , R_w, r_d, D_i, D_e, B_g, δ, B_{ry} , B_{sy}, N_s) must respect the following constraint:$x_{imin} \leq x_i \leq x_{imax}$. The values of the lower limit x_{imin} and the upper limit x_{imax} are established following technological, physical and expert considerations, for example:

- The internal and external diameter of the motor are delimited by the space reserved for the motor.
- The variation beaches of the wheel radius and nominal speed are defined starting from the Information Technology and schedule of conditions.
- The variation beaches of the flux density in the rotor yoke, the flux density in the stator yoke and in the air-gap are defined starting from the B-H curve of the iron to avoid the saturation problem.
- The current density is an expert data.
- The number of the phase spires is selected according to the energy stored in the batteries, the elementary voltage by battery and the space reserved to the batteries.

Another physical constraint results in the fact that the demagnetisation current must be higher than the maximal current and this not to demagnetize the magnets.

The optimisation problem can be expressed as follows:

$$\left\{\begin{array}{c} \text{maximise}(\text{EVP}) \\ with: \\ 500\leq f_{sw}\leq 5000\ (Hz) \\ 0.25\leq R_w 0.35\ (m) \\ 1\leq r_d\leq 8 \\ 562\leq T_d\leq 938\ \ (Nm) \\ 0.025\leq D_i\leq 0.25\ (m) \\ 0.26\leq D_e\leq 0.5\ (m) \\ 0.1\leq B_g\leq 1.04\ (T) \\ 0.1\leq B_{ry}\leq 1.06\ (T) \\ 0.1\leq B_{sy}\leq 1.6\ (T) \\ 10\leq N_s\leq 1000 \\ r\leq 10\% \\ Udc\leq 300\ (V) \\ I\leq I_d\,(A) \\ T_a\leq 50\ (°C) \\ T_b\leq 110\ (°C) \end{array}\right\} \tag{84}$$

Where T_d is the electric vehicle dimensioning torque (T_d=T_{dim}/r_d), T_a and T_b are respectively the magnets and the coils temperatures.

The EVP model is coupled to a program of optimization by the method of the genetic algorithm. The progress of the program of optimization of the EVP with constraints is

described by the organization diagram illustrated by figure 16 [14], [15], [16], [17], [18]:

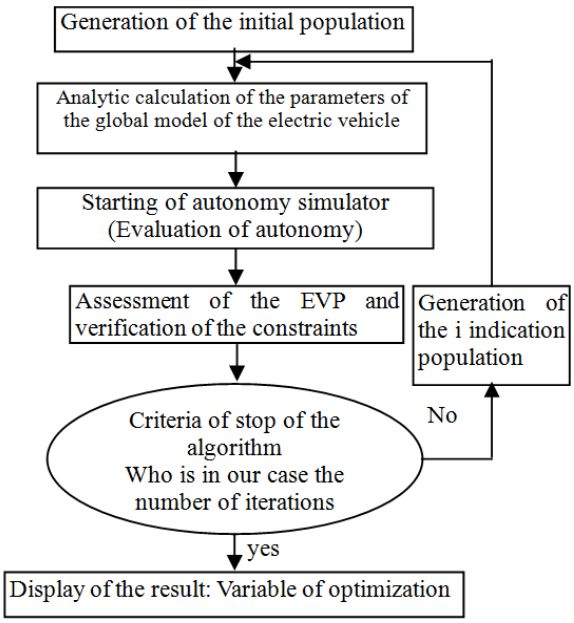

Figure 16. *Progress of the optimization program.*

13. Conclusion

An analytical and parameterized model sizing several configurations of permanents magnets motors and evaluating EVP was developed. This model takes in account of systems interactions and technological and physical constraints such as the computation of the continuous voltage of the DC bus at maximal speed. This design approach is validated by finite element method and experimental tests. The variation intervals of parameters influencing EVP are fixed after several simulations of the systemic design program with Matlab software version 7.1. In addition, a genetic algorithm optimizing these parameters is developed. Finally, the results presented in this paper are encouraging and opens the line of research on several projects such as the development and integration of electronic robust control laws. In conclusion, the traction chain conceived around parameters optimizing EVP and respecting the thermal, technological and physical constraints of the application, presents an interesting solution to the problem of electric vehicles production in great series.

List of Symbols

A_m	: Area of one magnet	m^2
A_t	: Area of one tooth	m^2
A_e	: Slot angular width	rad
A_d	: Tooth angular width	rad
B_g	: Flux density in the air-gap	Tesla
B_{min}	: Minimum flux density allowed in the magnets	Tesla
B_r	: Remanence,	Tesla
B_{ry}	: Flux density in rotor yoke	Tesla
B_{sy}	: Flux density in stator yoke	Tesla
c	: Core loss	/
d	: Density of the metal sheet	Kg/m^3
d_c	: Density of the copper	Kg/m^3
d_m	: Density of magnet	Kg/m^3
δ	: Current density	A/m^2
g	: Air-gap thickness	m
I	: Pick current powering the motor	A
$K_f < 1$	: Slot filling factor	/
$K_{fu} < 1$	: Magnet leakage coefficient	/
L_m	: Length of the stack of metal sheets(radial motor)	m
L_{sp}	: Average length of spire	m
λ	: Angle that the road makes with the horizontal	rad
μ_m	: Magnet relative permeability	/
μ_0	: Air permeability	/
n	: Modules number	
N_t	: Number of principal teeth	
r	: Undilation factor	/
N_s	: Number of spire per phase	/
Ω	: Angular speed of the motor	rad/s
U_{dc}	: Converter continuous voltage	Volt
r_d	: Gear ratio	/
D_m	: Bore diameter of the radial motor	m
r_p	: Loss coefficient in the totality reducer motor	/
r_{cu}	: Copper resistivity	ohm.m
S_c	: Copper active section	M^2
T	: Electrical period	s
W_a	: Angular width of the magnet	rad
D_e	:External diameter	m
D_i	:Internal diameter	m
T_m	:Electromagnetic torque	N.m
v	:Vehicle speed	m/s
M_v	:Vehicle mass	kg
R_w	:Vehicle wheel radius	m
J	:Motor moment of inertia	$Kg.m^2$
T_b	:Motor rubbing torque	N.m
T_{vb}	:Viscous rubbing torque of the motor	N.m
T_{fr}	: Fluid rubbing torque of the motor	N.m
T_r	:Torque due to the friction resistance	N.m
T_a	:Aerodynamic torque	N.m
T_c	:Climbing torque	N.m
T_d	:Reducer losses torque	N.m
s	:Dry friction coefficient	/
χ	:Viscous friction coefficient	/
k	:Fluid friction coefficient	/
P_f	:Iron losses	w
M_{va}	:Air density	Kg/m^3
A_f	:Vehicle frontal area	m^2
I_{dim}	:Dimensioning torque	N.m
t_m	:Magnet thickness	m
h_s	:Slot height	m
A_s	:Slot width	m
t_{ry}	:Rotor yoke thickness	m
T_{sy}	:Stator yoke thickness	m
P	:Number of poles pairs	/

R	:Phase resistance	ohm
L	:Phase inductance	H
W_t	:Tooth weight	kg
W_c	:Copper weight	kg
W_{ry}	:Rotor yoke weight	kg
W_{sy}	:Stator yoke weight	kg
W_m	:Magnets weight	kg
P_c	:Conduction losses	w
P_{com}	:Commutation losses	w
ρ	:Cyclic ratio	/
f_{sw}	:Switched frequency	Hz
V_{ce}	:Transistor collector-emettor voltage	Volt
V_d	:Diode terminal voltage	Volt
E_{on}	:Energy dissipated by commutation at the closing of IGBT	J
E_{off}	:Energy dissipated by commutation at the opening of IGBT	J
P_r	:Reducer losses	w
A_u	:Average autonomy	kg
η	:Traction chain efficiency	/
P_b	:Battery losses	w
P_{uml}	:Average power at wheels	w
v_m	:Average velocity of circulation mission	m/s
E_r	:Energy recovered by braking	kw.h
s_{slot}	: Slot area	m^2
T_{dim}	Dimensioning torque of the motor	Nm
T_d	Vehicle dimensioning torque	Nm

References

[1] Chaithongsuk, S., Nahid-Mobarakeh, B., Caron, J., Takorabet, N., & Meibody-Tabar, F. : Optimal design of permanent magnet motors to improve field-weakening performances in variable speed drives. Industrial Electronics, IEEE Transactions on, vol 59 no 6, p. 2484-2494, 2012.

[2] Rahman, M. A., Osheiba, A. M., Kurihara, K., Jabbar, M. A., Ping, H. W., Wang, K., & Zubayer, H. M. : Advances on single-phase line-start high efficiency interior permanent magnet motors. Industrial Electronics, IEEE Transactions on, vol 59 no 3, p. 1333-1345, 2012.

[3] C.C Hwang, J.J. Chang : Design and analysis of a high power density and high efficiency permanent magnet DC motor, Journal of Magnetism and Magnetic Materials, Volume 209, Number 1, February 2000, pp. 234-236(3)-Publisher: Elsevier.

[4] MI. Chunting CHRIS : Analytical design of permanent-magnet traction-drive motors" Magnetics, IEEE Transactions on Volume 42, Issue 7, July 2006 Page(s):1861 - 1866 Digital Object Dentifier 10.1109/TMAG.2006.874511.

[5] S.TOUNSI, R.NÉJI, F.SELLAMI : Conception d'un actionneur à aimants permanents pour véhicules électriques, Revue Internationale de Génie Électrique volume 9/6 2006 - pp.693-718.

[6] Sid Ali. RANDI : Conception systématique de chaînes de traction synchrones pour véhicule électrique à large gamme de vitesse. Thèse de Doctorat 2003, Institut National Polytechnique de Toulouse, UMRCNRS N° 5828.

[7] C. PERTUZA : Contribution à la définition de moteurs à aimants permanents pour un véhicule électrique routier. Thèse de docteur de l'Institut National Polytechnique de Toulouse, Février 1996.

[8] S. TOUNSI, R. NEJI and F. SELLAMI: Mathematical model of the electric vehicle autonomy. ICEM2006 (16th International Conference on Electrical Machines), 2-5 September 2006 Chania-Greece, CD: PTM4-1.

[9] R. NEJI, S. TOUNSI, F. SELLAMI: Contribution to the definition of a permanent magnet motor with reduced production cost for the electrical vehicle propulsion. Journal European Transactions on Electrical Power (ETEP), Volume 16, issue 4, 2006, pp. 437-460.

[10] P. BASTIANI : Stratégies de commande minimisant les pertes d'un ensemble convertisseur machine alternative : application à la traction électrique. Thèse INSA 01 ISAL 0007, 2001.

[11] G. Henriot : Traité théorique et pratique des engrenages : théorie et technologie 1. tome 1 Edition Dunod 1952.

[12] D-H. Cho, J-K. Kim, H-K. Jung and C-G. Lee: Optimal design of permanent-magnet motor using autotuning Niching Genetic Algorithm, IEEE Transactions on Magnetics, Vol. 39, No. 3, May 2003.

[13] Islam, M. S., Islam, R., & Sebastian, T. : Experimental verification of design techniques of permanent-magnet synchronous motors for low-torque-ripple applications. Industry Applications, IEEE Transactions on, vol 47 no 1, p. 88-95, 2011.

[14] Parasiliti, F., Villani, M., Lucidi, S., & Rinaldi, F. : Finite-element-based multiobjective design optimization procedure of interior permanent magnet synchronous motors for wide constant-power region operation. Industrial Electronics, IEEE Transactions on, vol 59 no 6, p. 2503-2514, 2012.

[15] Mahmoudi, A., Kahourzade, S., Rahim, N. A., & Ping, H. W. : Improvement to performance of solid-rotor-ringed line-start axial-flux permanent-magnet motor. Progress In Electromagnetics Research, 124, p. 383-404, 2012.

[16] Duan, Y., & Ionel, D. M. : A review of recent developments in electrical machine design optimization methods with a permanent-magnet synchronous motor benchmark study. Industry Applications, IEEE Transactions on, vol 49 no 3, p. 1268-1275, 2013.

[17] Liu, G., Yang, J., Zhao, W., Ji, J., Chen, Q., & Gong, W. : Design and analysis of a new fault-tolerant permanent-magnet vernier machine for electric vehicles. Magnetics, IEEE Transactions on, vol 48 no 11, p. 4176-4179, 2012.

[18] Lee, S., Kim, K., Cho, S., Jang, J., Lee, T., & Hong, J. : Optimal design of interior permanent magnet synchronous motor considering the manufacturing tolerances using Taguchi robust design. Electric Power Applications, IET, vol 8 no 1, 23-28, 2014.